HHS Public Access

Author manuscript

Int J Pharm. Author manuscript; available in PMC 2021 March 18.

Published in final edited form as:

Int J Pharm. 2020 December 15; 591: 119989. doi:10.1016/j.ijpharm.2020.119989.

Rational Design of Multistage Drug Delivery Vehicles for Pulmonary RNA Interference Therapy

A. Sofia Silva[a,b,c,1,*], **Kevin E. Shopsowitz**[b,c,2], **Santiago Correa**[b,c,3], **Stephen W. Morton**[b,c], **Erik C. Dreaden**[b,c,4], **Teresa Casimiro**[a], **Ana Aguiar-Ricardo**[a,*], **Paula T. Hammond**[b,c,d,*]

[a]LAQV-REQUIMTE, Departamento de Química, Faculdade de Ciências e Tecnologia, Universidade NOVA de Lisboa, 2829-516 Caparica, Portugal

[b]Koch Institute for Integrative Cancer Research, Massachusetts Institute of Technology, Cambridge, Massachusetts 02139, United States

[c]Department of Chemical Engineering, Massachusetts Institute of Technology, Cambridge, Massachusetts 02139, United States

[d]Institute for Soldier Nanotechnologies, Massachusetts Institute of Technology, Cambridge, Massachusetts, 02139, United States

Abstract

Small interfering RNA (siRNA) therapy has significant potential for the treatment of myriad diseases, including cancer. While intravenous routes of delivery have been found to be effective for efficient targeting to the liver, achieving high accumulations selectively in other organs, including lung tissues, can be a challenge. We demonstrate the rational design and engineering of a layer-by-layer (LbL) nanoparticle-containing aerosol that is able to achieve efficient, multistage delivery of siRNA *in vitro*. For the purpose, LbL nanoparticles were, for the first time, encapsulated in composite porous micro scale particles using a supercritical CO2-assisted spray drying (SASD) apparatus using chitosan as an excipient. Such particles exhibited aerodynamic properties highly favorable for pulmonary administration, and effective silencing of mutant KRAS in lung cancer cells derived from tumors of a non-small cell lung cancer (NSCLC) autochthonous model. Furthermore, efficient alveolar accumulation following inhalation in healthy mice was also observed, corroborating *in vitro* aerodynamic results, and opening new perspectives for further studies of effective lung therapies These results show that multistage aerosols assembled by supercritical CO_2-assisted spray drying can enable efficient RNA interference therapy of pulmonary diseases including lung cancer.

* sofiamsilva@ua.pt; air@fct.unl.pt; hammond@mit.edu.

[1]Current affiliation: CICECO, Department of Chemistry, University of Aveiro, 3810193, Aveiro, Portugal

[2]Current affiliation: Faculty of Medicine, University of British Columbia, BC V1Y 1T3, Canada

[3]Current affiliation: Department of Materials Science and Engineering, Stanford University, 496 Lomita Mall, Stanford, CA 94305, USA

[4]Current affiliation: Wallace H. Coulter Department of Biomedical Engineering, Georgia Institute of Technology and Emory University, Atlanta, GA, 30332, United States. Department of Pediatrics, Aflac Cancer and Blood Disorders Center, Children's Healthcare of Atlanta, Emory University School of Medicine, Atlanta, GA, 30332, United States.

Conflict of Interest: The authors declare no competing financial interest.

Supplementary material

Supplementary data to this article can be found online.

Keywords

layer-by-layer nanoparticles; small interfering RNAs; pulmonary delivery; micronized systems; supercritical carbon dioxide

1. Introduction

Small interfering RNAs (siRNAs) have potential applications in several medical conditions that range from cancer to neuromuscular disorders. Clinical trials using siRNA to knockdown particular proteins in certain diseases and disorders have recently been performed,(Conde et al., 2015; Merkel et al., 2014) and Patisiran, a first commercial intravenous lipidic siRNA nanoparticle to treat Hereditary ATTR amyloidosis(Morrison, 2018) just got FDA approval.("FDA approves first-of-its kind targeted RNA-based therapy to treat a rare disease," 2018) Nevertheless, the delivery of functional siRNA to target cells remains a key challenge. Nucleic acids are not suitable for systemic administration, due to their poor pharmacokinetics and low stability. Unmodified siRNA is rapidly degraded by endonucleases in the bloodstream (Conde et al., 2015; Okuda et al., 2013) moreover, intracellular delivery of siRNA, even in more stabilized forms, to target cells is challenging due to charge-charge repulsion with cellular membranes and a lack of efficient mechanisms to enable the cellular uptake of nucleic acids and subsequent trafficking to the cytosol.(Jere et al., 2009; Malmsten, 2013; Merkel et al., 2014; Okuda et al., 2013) To overcome these barriers, a number of formulations that compact siRNA into nanoscale systems suitable for cellular internalization have been widely investigated for *in vitro* and *in vivo* applications. (Merkel et al., 2014) Among these, the ability to self-assemble siRNA into electrostatically assembled layer-by-layer (LbL) nanoparticles are promising due to their simplicity, scalability, and use of highly biocompatible polyelectrolytes to achieve controlled release. (Zhou J. Deng et al., 2013) These nanometer-scale particles serve as a modular drug delivery platform that can be adapted to dual or monotherapies, and can carry siRNA effectively to the target site and release it intracellularly and in a sustained fashion.(Zhou J. Deng et al., 2013; Hartmann et al., 2013) The local and controlled delivery of siRNA is of major clinical importance, since it circumvents the potentially undesirable side effects of high systemic therapeutic doses, such as nonspecific tissue accumulation.(Hartmann et al., 2013)

Lung cancer, including non-small cell lung cancer (NSCLC) and small cell lung cancer (SCLC), among both men and women worldwide is one of the top 10 global causes of death. ("The top 10 causes of death," 2018) The most frequent NSCLC subtype is lung adenocarcinoma, which often results from activating mutations in Kirsten rat sarcoma viral oncogene homolog (KRAS) (~20-30%), TP53 (~50%), and others. Hence, the targeted inhibition of KRAS expression and stimulation of p53 effector functions are promising treatments for this particular lung cancer. However, direct and specific KRAS inhibition by small-molecule compounds is still elusive. Consequently, KRAS is a promising candidate for siRNA-based therapy, which can treat such 'undruggable' diseases by downregulating the expression of the target gene in a post-transcriptional manner.(Xue et al., 2014a) For instance, Xue and co-workers have already demonstrated that oncogenic RAS can play a crucial role in tumor maintenance and that siRNA may effectively inhibit this gene.(Xue et

al., 2014b) In prior work, we systemically delivered nanoparticles containing siRNA and microRNA (along with cisplatin) to target KRAS and replace p53 effector function, respectively.(Gu et al., 2017)

Chemotherapeutics may be administered to the lung systemically, which requires routing through the blood stream and significant clearance to liver and spleen; alternatively, effective siRNA delivery to the lungs can also be achieved through pulmonary administration(Dufort et al., 2015; Taratula et al., 2011; Xue et al., 2014b). Such local delivery enables the administration of lower siRNA doses than required for systemic delivery, as a larger fraction of delivered therapeutic can reach its target, thereby decreasing potential side effects and improving patient compliance via self-dosing.(Gu et al., 2017; Lam et al., 2012; Youngren-ortiz et al., 2017) Although the pulmonary delivery of drugs can be achieved through inhalation via intranasal and intratracheal routes, the former is considered clinically superior as it provides a large absorptive surface for aerosol deposition, allowing the drugs to avoid first pass metabolism.(Silva et al., 2014a) To ensure effective delivery, however, major barriers such as degradation by RNase, mucociliary, cough and alveolar macrophage clearances must be overcome.(Feldmann and Merkel, 2015; Merkel et al., 2014; Youngren-ortiz et al., 2017) The particle's aerodynamic diameter also poses a major challenge to efficient particle deposition in the deep lung. Nanoscale particles are prone to exhalation and the ideal aerodynamic diameter for deep lung deposition ranges from 1-5 μm.(Cabral et al., 2016; Restani et al., 2016; A. S. Silva et al., 2017; M. C. Silva et al., 2017) While microscale particles exhibit optimal accumulation in the deep lung, they also show poor cellular uptake compared with nanometer scale particles. Thus, technologies that achieve multistage delivery could improve the delivery of siRNA to diseased cells within lung tissues.(Chow et al., 2017; Okuda et al., 2013)

$ScCO_2$-assisted processes for the production of dry powder formulations have been successfully implemented.(Restani et al., 2016; A. S. Silva et al., 2017) Likewise, this technology has already been successfully applied to produce powders of nucleic acids, such as siRNA for inhalable gene delivery. Okuda et al. prepared a chitosan/siRNA dry powder via a $scCO_2$ antisolvent method and established a powerful and specific *in vivo* gene silencing effect following pulmonary administration in mice. The resulting spike-like powders, however, had to be manually ground before successful administration to the mice. Neither flowability tests nor release assays investigated the release rate of siRNA from the powders.(Merkel et al., 2014; Okuda et al., 2013)

In the current study, we have engineered dry powder siRNA inhalable systems targeting mutant KRAS in lung adenocarcinoma on a laboratory scale SASD apparatus. Chitosan (CHT), a natural polysaccharide generally thought to be biocompatible and biodegradable, (Al-Qadi et al., 2012; Cabral et al., 2016; Restani et al., 2016; A. S. Silva et al., 2017) was selected as a microparticle carrier. SADS technology enabled us to produce clean, ultrafine dry powder formulations with suitable aerodynamic diameters and morphology for pulmonary delivery.(Cabral et al., 2016; Restani et al., 2016; A. S. Silva et al., 2017; Tavares et al., 2017) LbL nanoparticles were developed as film carriers to ensure the controlled release of the siRNA and guarantee it remain stable until delivery. Due to their biodegradable and biocompatible features and the ability to serve as a reservoir for key

biomolecules(Maggini et al., 2016), mesoporous silica nanoparticles (MSN) were used as the assembly core, while poly-L-arginine (PLR) was used as the polycation and hyaluronic acid (HA), as the polyanion in the outermost layer of the nanoparticle, respectively (Figure 1A). HA facilitated cell-specific delivery, due to the binding of HA CD44 receptors overexpressed in NSCLC.(Gu et al., 2017) Such targeted constructs will enable specific binding to tumor cells in the lung and controlled siRNA release, once CHT is degraded by the airway mucus and lining fluid enzymes, allowing diffusion of its content through the microparticle pores.(Domínguez-delgado et al., 2014; Grenha et al., 2010; Jae et al., 2006; Temtem et al., 2012) The combined formulations were fully characterized regarding their morphological properties, gene silencing efficiency, biocompatibility, and aerodynamic features. An *in vitro* pharmacokinetic study was carried out, followed by *an in vivo* biodistribution proof-of-concept assay, by aerosol inhalation of the powders in healthy mice, to demonstrate the ability of our nano-in-micro particles, produced by this greener and innovative technology, in attaining the region of pulmonary alveolus. Scheme 1 displays a schematic representation of all the experiments performed.

2. Experimental Section

2.1. Materials

Stable tdTomato expressing KP derived lung adenocarcinoma lines (KP cells) were previously synthetized by Wen and co-workers(Xue et al., 2014b) KRAS 1211 modified siRNA (5’-UAAAGUCUAGGACACGCUGUUUU-3’) was purchased from Dharmacon. AllStars negative Alexa Fluor 488 siRNA (AF 488 siRNA) was acquired from Qiagen. Silencer Negative Control siRNA (NC siRNA), NucBlue Live ReadyProbes Reagent (Hoechst 33342) and Lipofectamine® 2000 Transfection Reagent were purchased from ThermoFisher Scientific. Corning 384 flat bottom black polystyrene low volume/flat microplate were kindly provided by Corning Corporation. QuantiGene RNA assay and KRAS and MRPL53 reference genes were bought from Affymetrix. RNA ladder was purchased from NEB. Hollow fiber module 300 kDa modified polyethersulfone (mPES) was supplied by Spectrum Labs. Hyaluronic acid (HA, 40 kDa) was purchased from Lifecore Biomedical. CellTiter Glo kit was procured from Promega. Heparin sodium (PH-3005) came from Celsus laboratories. Dulbecco’s modified eagle’s medium F12 (DMEM F12), Fetal bovine serum (FBS) and penicillin/spectromycin were purchased from Media Tech. Ribogreen assay and RNAse free water were acquired from Life Technologies. IR-780 iodide dye, poly-L-arginine (PLR, 5-15 kDa), hyaluronidase from bovine testes type VIII (Hdase), proteinase K from Tritirachium album (Pkase), lysozyme chloride from Grade VI: from chicken egg white, tetraehtyl orthosilicate (TEOS), trimethylamine, cetyltrimethylammonioum bromide (CTAB), methanol (MeOH), phosphate buffer saline (PBS), dibasic sodium phosphate, citric acid and sodium citrate were purchased from Sigma-Aldrich. Optimum cutting temperature (O.C.T.) fixing agent was bought from Sakura Finetek. Acetic acid glacial (99.7 % purity) was acquired from Carlo Erba Reagents. Ethanol absolute anhydrous (99.9 % purity) was sourced from Scharlau. Chitosan (viscosity 5-20 mPa.s, 0.5 % in 0.5 % acetic acid at 20 C) came from Tokyo Chemical Industry. Hydranalcoulomat AD was also from Sigma-Aldrich and was used in Karl Fischer. Dry powder insufflator was purchased from Penn Century. All components were used as received

without any further purification. Industrial carbon dioxide (purity 99.93 %) from Air Liquid was used.

2.2. Preparation of IR-780 loaded mesoporous silica nanoparticles (MSNs)

MSNs were synthesized by adapting the several methods described in the literature for the synthesis of this type of nanoparticle.(Moreira et al., 2014; Zhang et al., 2013) Briefly, 4.2 mmol of CTAB and 2.3 mmol of triethanolamine were mixed with 100 mL of H_2O and heated at 80 °C (until dissolved). Then, 70 mmol of TEOS were quickly added and the solution was stirred for 1 hour. The particles were isolated by high speed centrifugation (30,000 x g, 30 min) and washed once with water and once with MeOH. Particles were resuspended in 200 ml of MeOH, followed by the addition of 2 mL of 12 M HCl. The suspension was refluxed at 80 °C for 14 h and the particles were recovered by centrifugation (30,000 x g, 30 min), followed by two washes with methanol. IR-780 iodide is a near-infrared (NIR) fluorescence dye with great importance in theragnosis.(Yue et al., 2013) This dye was loaded into MSN to monitor nanoparticles entrapment efficiency into CHT microspheres. IR-780 dye loading was accomplished using solvent evaporation with slight modifications. To load the dye in the pores of the particles, 90 mg of MSN were soaked in a concentrated solution of the dye (2 mg/mL in MeOH), with the aid of an ultrasonic bath, and the procedure was repeated 3 times. The solvent used for the dye dissolution was evaporated after each impregnation, under reduced pressure, in order to more completely fill the dye pores and improve the loading efficiency of the nanocarriers.(Moreira et al., 2014) Following the last procedure, the particles were washed with 500 μL of ultrapure water to remove the IR-780 dye not loaded into the MSNs. The particles were recovered by high-speed centrifugation (30,000 x g, 15 min). The resulting particles were recovered and dried under reduced pressure overnight. The amounts of loaded and unloaded dye were quantified by measuring particles and their supernatant fluorescence in a microplate reader (Infinite 200 from Tecan,) and compared against a calibration curve.

2.3. siRNA Layer by Layer (LbL) assembly nanoparticles

The nanoparticle LbL assembly was developed on the basis of the previously established methods, with slight modifications.(Correa et al., 2016, 2015; Zhou J Deng et al., 2013; Dreaden et al., 2015) For LbL assembly, 5 mg of MSN_IR-780 were redispersed in 10 mL of 2 mM PBS (pH 7.4). A solution of 1.5 mg/mL of the polycation PLR (5 – 15 kDa) in RNAse free water was added dropwise to the nanoparticles' dispersion, under stirring. The solutions were allowed to mix for 30 sec more in an ultrasonic bath, followed by purification in a bench scale tangential flow filtration (TFF) development systems with data acquisition and pressure indicator (Spectrum Labs KrosFlo Researcher II). This filtration was performed using a 300 kDa modified polyethersulfone hollow fiber module (Spectrum Labs MidiKros D02-E300-05-N) at a flow rate of 200 mL/min (no pressure applied). A total of 4 washes were performed. To incorporate siRNA, purified nanoparticles were mixed with a siRNA solution (in RNase free water) containing a mixture of a KRAS siRNA and AF 488 siRNA (120 nmol and 16 nmol, respectively). Control samples containing NC siRNA and AF 488 siRNA were also prepared in the same proportions for control purposes. Again, the siRNA mixture was added dropwise to the purified nanoparticles, under stirring. Once more, the solutions were sonicated for an extra 30s to allow particles–siRNA interaction/collision.

Again, the particles were purified using another 300 kDa modified polyethersulfone hollow fiber module at a flow rate of 200 mL/min (no pressure applied). The purified polycation/siRNA nanoparticles were further mixed with a new solution of 1.5 mg/mL of the polycation PLR (5 – 15 kDa) in RNAse free water. The adding and purification procedure were the same as described above. Finally, the resulting particles were layered with a previously chilled (4 °C) hyaluronic acid (HA) (40 kDa) solution (2 mg/mL) containing 100 nM dibasic sodium phosphate (pH 7.4). The HA solution was added in a single, strong and efficient manner to the purified nanoparticles placed in an ultrasonic bath, and placed at 4 °C for 30 min. Further purification was performed using the same type of hollow fiber modules at a flow rate of 140 mL/min with a pressure of 0.07 MPa. (Correa et al., 2016, 2015)

2.4. Physicochemical characterization of the LbL assemblies

2.4.1. Size, charge and uniformity measurements of LbL nanoparticles—

All size, zeta potential and polydispersity index measurements were performed using a Malvern ZS90 zeta-sizer in PBS 2mM. Transmission electron microcopy (TEM) was assessed using a JEOL 2010 FEG Analytical Electron Microscope (JEOL). Samples were prepared by drop casting nanoparticle suspensions onto carbon coated copper grids without any staining.

2.4.2. Measurement of encapsulation efficiency of siRNA in LbL nanoparticles using Ribogreen—

The encapsulation efficiency of siRNA on the LbL nanoparticles was performed using a Ribogreen assay. For the purpose, two approaches were tested: 1) the total layered siRNA was measured using a Ribogreen immediately after siRNA deposition on the surface of MSN_IR-780/PLR; 2) the total siRNA was accessed after LbL nanoparticles formation following enzymatic digestion using specific enzymes to digest HA (hyaluronidase)(Choi et al., 2010) and PLR (Proteinase K),(Zeng et al., 2004). After the addition of a heparin solution (to compete for the siRNA), Ribogreen was used to quantify the total siRNA. In addition, the siRNA integrity was evaluated through electrophoresis in an agarose gel.

2.4.3. Measurement of encapsulation efficiency of siRNA in LbL nanoparticles using AlexaFluor 488 labeled siRNA—

The encapsulation efficiency of AlexaFluor 488 siRNA on the LbL nanoparticles was also examined by measuring the amount of fluorescent siRNA 1) immediately after siRNA layering, and 2) after the enzymatic degradation of HA and PLR of the LbL nanoparticles and heparin addition. Both experiments were compared against a standard curve.

2.4.4. Measurement of siRNA release from LbL nanoparticles using Ribogreen—

The siRNA release assays were evaluated using 3 different buffer solutions: PBS solution at pH 7.4 to mimic cells' physiological pH, phosphate buffer saline solution at pH 6.8 to mimic the extracellular environment of cancer cells, and citrate buffer solution, pH 5.5 to mimic the endosomal environment of cancer cells. (Caruso et al., 2012; Webb et al., 2011; Xu et al., 2015b, 2015a) The release assays were performed in the following manner: 500 μL of nanoparticle suspension (n = 3, for each pH) were centrifuged at high speed (30,000 x g, 15 min). The supernatant was recovered and stored for siRNA quantification. The nanoparticles were redispersed in 1 mL of each buffer solution and the siRNA released

from the microparticles was evaluated for 3 days, with the aid of Ribogreen quantification assay, according to manufactures' instructions. Prior to Ribogreen quantification, heparin (10 mg/mL) was added to compete for the siRNA released to the medium.(Krieg et al., 2014)

2.5. Preparation of CHT-LbL siRNA Powders by Supercritical Assisted Spray Drying (SASD)

Dry CHT-LbL siRNA and dry CHT-MSN powders were prepared based on the SASD method, as previously described with slight modifications.(Cabral et al., 2016; Restani et al., 2016; A. S. Silva et al., 2017) As we were only addressing the biodistribution of the developed powders in lung mice, both siRNA LbL nanosystems (KRAS 1211 modified siRNA and NC siRNA) were combined in order to enhance the amount of fluorescent siRNA for a more accurate biodistribution panel. The LbL assemblies were centrifuged at high speed (30,000 x g, 30 min) and the resultant pellet (10 mg of nanoparticles) was placed in a casting solution of chitosan (CHT) (1 % w/v) prepared in 1 % of acid water and 20 % (v/v) of ethanol and homogenized under stirring. Liquefied CO_2 was pumped with a high-pressure liquid pump (HPLC pump K-501, Knauer), which was then heated and sent to the static mixer (model 37-03-075, Kenics-Chemineer, 4.8 mm ID x mm L, 27 helical mixing elements). The casting solution containing both nanoparticles and CHT was pressurized through a high-pressure pump (HPLC 305, Gilson) to the static mixer that provided a near-equilibrium mixing of $scCO_2$ and the liquid solution. Pressure was measured with a Setra pressure transducer (0.1 psig stability). The solution was then sprayed through a 150 μm diameter nozzle into a thermostated aluminum precipitator (± 0.1 °C), operating at near atmospheric pressure, where particles were formed by drying the droplets using a heated air flow (70 °C). The formed particles exited the precipitator at the bottom and passed into a cyclone where they were separated from the gas stream and collected into a reservoir. (Cabral et al., 2016) Tmix = 70 °C; Tpreci = 90 °C; pCO_2 = 10 MPa

2.6. Characterization of microparticles

Particle size (sieve and Feret's diameter) was determined using an optical particle analyzer system (Morphologi G3 Essentials, from Malvern Instruments Ltd). The particles were characterized by the volume mean diameter (Dv) and the relative width of the distribution (Span), calculated as follows:

$$Span = \frac{D_{v,90} - D_{v,10}}{D_{V,50}} \quad \text{Eq.1}$$

where $D_{v,90}$, $D_{v,10}$ and $D_{v,50}$ were the diameters at 90 %, 10 % and 50 % cumulative volume. To observe morphology, the microparticles were imaged via scanning electron microscopy (SEM) (JEOL) at various amplifications. All the samples were mounted on aluminum stubs using carbon tape and were sputter-coated with 5 nm Pt/Pd. (Cabral et al., 2016)

X-ray powder diffraction (XRD) analysis was performed in a RIGAKU X-ray diffractometer (model Miniflex II). Samples were placed in a holder and analyzed through CuKα radiation (30 KV/15 mA), with a 2θ angle ranging between 2° and 55° with a scan rate of 1°/min.

Moisture content of each formulation was assessed using Karl Fischer assay (Metrohm). 1.5 mg of powder were accurately weighed and introduced in the reaction cell. Moisture content was determined by subtracting the background signal.(Amidi et al., 2008; Cabral et al., 2016; Naikwade et al., 2009; Restani et al., 2016)

Surfaces areas were calculated by the Brunauer Emmett Teller (BET) method and were determined in a Micromeritics ASAP 2010 Physisorption Analyzer, using 50 mg of samples. The analysis was performed in two phases, first by heating the sample to 320 K for 42 h in order to release all adsorbed gases in the particle. Secondly, the temperature was lowered and kept at 77.35 K throughout analysis. (Cabral et al., 2016)

LbL siRNA nanoparticle distribution among CHT microparticles was evaluated through different techniques. Fluorescent siRNA spreading onto CHT microparticles was analyzed using Olympus FV1200 Laser Scanning Confocal (Olympus). Scanning TEM (STEM) and energy dispersive X ray spectroscopy (EDX) maps were simultaneously recorded using JEOL 2010 FEG Analytical Electron Microscope (JEOL), with the aid of Gatan Digital Micrograph software. The combination of these techniques enabled us to visualize the surface of the solid template (microspheres) and assign specific elemental peaks.

Entrapment Efficiency.—Entrapment efficiency was determined by measuring the amount of IR-780 dye presented in the powders. Briefly, 1 mg of CHT-LbL siRNA powders were dissolved in water and IR-780 dye fluorescence was assessed in a microplate reader. The entrapment efficiency (E%) of IR-780 dye was calculated as follows:

$$E\,\% = \frac{m_r}{m_i} \times 100 \qquad \text{Eq.2}$$

where mr was the amount of IR-780 dye remaining within the particles and mi represents the IR-780 dye presented in the LbL assemblies loaded into the casting solution. This percentage matched the percentage of the whole LbL nanosystems entrapped.

2.7. *In vitro* aerosolization study

An *in vitro* dry powder aerosolization study was carried out for the CHT-MSN formulations using seven stages Andersen Cascade Impactor (ACI) (Coopley Scientific). In a typical procedure, 30 mg of powder were loaded into 5 hydroxypropylmethylcellulose capsules (Aerovaus), which were individually placed in a handheld, dry powder, breath activated inhaler (AerolizerTM plastique 60LPM, model 7), previously weighed, which was coupled to the ACI device. The 7 metal plates within the cascade impactor were covered with pre-weighted glass microfiber filters (MFV1 diameter 80 mm, Filter Lab). The DPI punctured the capsule prior to inhalation and a high capacity pump was activated to simulate inspiration: air flow rate 60 L/min during 4 s, according to the European pharmacopeia. (Council of Europe, 2010) The Cascade Impactor measurements were obtained by dispersing 4 consecutive capsules (n = 3). After dispersion, the filters and the dry powder inhalers (DPI) were weighed again. The dose (ED %), which corresponds to the total loaded powder mass exiting the capsules and inhaler, was determined gravimetrically and can be expressed as follows:

$$ED(\%) = \frac{m_{full} - m_{empty}}{m_{powder}} \times 100 \quad \text{Eq.3}$$

where m_{full} and m_{empty} are the weights (mg) of the capsule before and after simulating the inhalation, and m_{powder} is the initial weight (mg) of the powder in the capsule.

The Fine Particle Fraction (FPF) was determined by the interpolation of the percentage of the particles with less than 5 μm diameter emitted from the capsules in each ACI experiment. The Mass Median Aerodynamic Diameter (MMAD) was determined as the particle diameter corresponding to 50 % of the cumulative distribution. The Geometric Standard Deviation (GSD) was determined by the following equation:

$$GSD = \sqrt{\frac{d_{84}}{d_{16}}} \quad \text{Eq.4}$$

where d84 and d16 are the geometric diameters corresponding to 84 % and 16 % of the cumulative distribution, respectively.

2.8. Measurement of LbL nanoparticle release from microparticles

The release of LbL assemblies from the microparticles was evaluated at two distinct pHs: 7.4) and 6.8. Approximately 3 mg of the powders were transferred to a special membrane size cut off 1 μm and incubated in 1.5 mL of different pH solutions in a shaking (35 rpm) water bath at 37 °C. At pre-determined end points, the solutions were removed and replaced with 1.5 mL fresh buffer solutions. The removed solutions were centrifuged at 30,000 x g for 15 min and the supernatant was discarded. Afterwards, 50 μL of water was added to resuspend the pellet. The samples were placed in a 384 Well Black with Clear Flat Bottom Polystyrene and the spectrophotometer microplate reader was read. From the fluorescence obtained and from the amount of IR-780 dye initially entrapped in the microparticles, we were able to estimate the amount (%) of LbL nanoparticles being released from the micropowders. Nanoparticles released from swelling-controlled systems are modeled by the Korsmeyer-Peppas equation as follows:

$$\frac{M_t}{M_\infty} = kt^n \quad \text{Eq.5}$$

where M_t/M_∞ is the fraction of the drug released at time t, k is the rate constant and n is the diffusional exponent. The n-value is obtained from the slope of the Korsmeyer-Peppas plot and represents different release mechanisms. For spherical geometries: n = 0.43 for Fickian diffusion; 0.43 < n < 0.85 for anomalous non-Fickian diffusion; n = 0.85 for Case-II transport.(Ritger and Peppas, 1987; Siepmann and Siepmann, 2008)

2.9. Measurement of siRNA release from microparticles

The release of siRNA from the microparticles was also evaluated at two distinct pHs: 7.4) and 6.8 and following the exact same conditions above mentioned: 3 mg of the powders were transferred to a special membrane size cut off 1 μm and incubated in 1.5 mL of

different pH solutions in a shaking (35 rpm) water bath at 37 °C. At determined time points, 1.5 mL of buffer solutions were removed and replaced with fresh 1.5 mL of buffer solutions. The removed buffer was centrifuge and the pellet was discarded. To the removed supernadant,100 μL of a heparin solution (10 mg/mL) was added in order to compete for the siRNA. Afterwards, a Ribogreen assay quantified the amount of siRNA released from the microspheres.

The siRNA released from swelling-controlled systems was also modeled by the Korsmeyer-Peppas equation as above described.

2.10. *In vitro* performance of nano and nano-in-micro systems

KP tdTomato expressing cells were used in our experiments and grown in DMEM media supplemented with 10 % v/v heat-inactivated fetal bovine serum (FBS) and 1 % of antibiotic-antimycotic (penincilin G (100 U/mL)), spectromycin G (100 μg/mL)) at 37 C, under 5 % CO_2 humidified atmosphere.(Connor et al., 2005)

Gene silencing of siRNA LbL nanoparticles was assessed in KP tdTomato-expressing cell line. Briefly, the cells were seeded on a 96-Well plate overnight at a density of 1.2 x 10^4 cells/well, and treated with increasing concentrations of LbL nanoparticles of which the amounts were normalized to the siRNA loading - 10 and 100 nM (approximately 26 and 260 ng of siRNA KRAS). The cells were treated with KRAS-targeting siRNA LbL nanoparticles, and compared with NC siRNA nanoparticles and lipofectamine controls. Three days after treatment, cellular expression was evaluated through the QuantiGene RNA assay, according to the manufacturer's instructions. KRAS was used as the target gene and MRPL 53 was used as a reference gene. LbL nanoparticles containing negative control (NC) siRNA achieved less than 30 % gene silencing.

The experiment was repeated for the microformulations. The amount of powders administered was normalized to the amount of siRNA encapsulated. For this, two different concentrations of powders in solution were used: 0.6 mg/mL and 0.15 mg/mL, for either CHT or CHT-LbL siRNA microparticles (25 and 100 ng of siRNA KRAS, respectively).

Cytotoxicity assays were performed using CellTiter Glo, according to the manufacturer's instructions. Briefly, cells were seeded in a 96-well plate at a density of 1.2 x 10^4 cells/well for 24 h. Afterwards, they were treated with the nanoparticles at various concentrations (normalized to siRNA concentrations: 10 and 100 nM). Cellular ATP was monitored at 24 h and 72 h of incubation by replacing the medium by 100 μL of fresh media and 20 μL of the reagent mixture. Cell viabilities were normalized to an untreated control. The same procedure was repeated for the CHT-LbL siRNA powders. Again, the amount of powders administered was normalized to the amount of siRNA encapsulated and was the same as for the gene silencing assay. Cellular uptake of nanoparticles was assessed by confocal microscopy and flow cytometry. The confocal microscopic images were taken using an Olympus FV1200 Laser Scanning Confocal. Briefly, KP tdTomato cell line was seeded at a density of 1.2 x 10^4 cells/well on glass bottom dishes coated with collagen with 1 mL of DMEM supplemented with 10 % of FBS, during 24 h at 37° C, under 5 % CO_2 humidified atmosphere. Afterwards LbL nanoparticles were placed in contact with cells. One and 4h

after, the medium was replaced by DMEM supplement with 10 % of FBS and 1 % of antibiotic-antimycotic, and the cells were imaged. Further 3D reconstruction was performed using Imaris Bitplane (Vs7.6.1, Bitplane). The quantity of uptake was measured by flow cytometry. Briefly, the cells were seeded in a 48-well plate at a density of 50 x 10^4 cells/well with 1 mL of DMEM supplemented with 10% of FBS, during 24 h at 37° C, under 5 % CO_2 humidified atmosphere. Then, cells were treated with LbL fluorescently labeled nanoparticles at a concentration of 100 μg/mL for 1 and 4 h, followed by washing and trypsinization. The cell-associated fluorescence was analyzed by a BD LSRFortessa flow cytometer (BD Biosciences).

Microparticles' interactions with cells were carried out by seeding cells in glass bottom dishes coated with collagen at a density of 4 x 10^3 cells per well, for 24 h. Afterwards, nano-in-micro formulations were placed in contact with cells for 1 and 12 h and their interactions were imaged.

2.11. *In Vivo* proof-of-concept experimentation

Female BALB/c mice (4-6 weeks old) were purchased from Taconic, and the AIN-93 purified diet was from PharmaServ/Testdiets. Mice were kept on the AIN-93 diet for at least a week before experimentation to reduce levels of body autofluorescence. All *in vivo* experimentation was carried out under the supervision of the Division of Comparative Medicine (DCM), Massachusetts Institute of Technology, and in compliance with the Principles of Laboratory Animal Care of the National Institutes of Health. Mice were divided into 4 groups: i) untreated; ii) treated with CHT-LbL siRNA (30 min); iii) treated with CHT-LbL siRNA (24 h); treated with CHT powders (24 h). Prior to receiving the administration of the powder, the mice were anesthetized with isoflurane and held on their back. The trachea was exposed to a dry powder insufflator for mouse (Penn Century) and 1.5 mg of powder (2.8 μg of siRNA) was administered through the trachea. At pre-determined times, the mice were sacrificed and lung fluorescence derived from Alexa 488 siRNA (λ_{ex}= 465 nm ; λ_{em}: 520 nm) was detected using a Xenogen IVIS Imaging System (Caliper Instruments). Imaging and biodistribution data were normalized to the autofluorescence of the untreated mice. Further biodistribution analyses were performed both using confocal microscopy (Olympus FV1200 Laser Scanning Confocal) and two photon correlation microscopy with the aid of Olympus FV1000 Multiphoton Laser Scanning Confocal Microscope (Olympus) for deep tissue imaging of the lung, using a 25 x, N.A. 1.05 objective at 840 nm. Untreated lungs from healthy mice were also imaged in order to normalize lung autofluorescence. Both untreated lungs and the lungs of mice receiving black CHT microparticles were used as controls. *In vivo* serum toxicity of the CHT-LbL siRNA powders was assessed using serum from both the treated and control mice at the end of the experiment. Blood biochemistry of liver and kidney panels was analyzed by Charles River Laboratories. Lung tissues were fixed with O.C.T. and processed by the Swanson Biotechnology Histology Facility Core. The samples were sectioned for H&E staining. Sectioned images were collected using a Nikon light microscope, an Olympus FV1200 Laser Scanning Confocal and an Olympus FV1000 Multiphoton Laser Scanning Confocal Microscope.

2.12. Statistical analysis.

All statistical analyses, unless noted, (GraphPad Prism and Origin) were performed using one-way ANOVA analysis of variance following the Bonferroni post-hoc test with a significant set at $p < 0.05$.

3. Results and Discussion

3.1. Physicochemical characterization of aerosolizable LbL nanoparticles

Mesoporous (MSN) silica nanoparticles served as a scaffold for the LbL assembly of siRNA. To monitor nanoparticle entrapment in CHT microspheres, the IR-780 iodide was loaded into the MSN by solvent evaporation.(Moreira et al., 2014) Based on previous studies of the controlled release of siRNA using LbL nanoparticles, the architecture developed for these studies consisted of 4 layers – a polycation, adsorbed directly onto the negatively charged silica surface, followed by siRNA, then a terminal polycation/polyanion bilayer.(Zhou J. Deng et al., 2013) We used poly-L-arginine (PLR) as a polycation layer due to its propensity to enable endosomal escape,(Zhou J Deng et al., 2013) and hyaluronic acid (HA) served as the outermost polyanion layer since it specifically binds to the CD44 receptors overexpressed on lung adenocarcinoma cells and has been previously reported to show enhanced *in vivo* stability and plasma half-life.(Zhou J Deng et al., 2013; Gu et al., 2017) The (PLR/siRNA/PLR/HA) LbL coatings were assembled onto IR780-labeled MSNs (32 nm HD, −32.2 mV) via sequential adsorption, followed by tangential flow filtration (TFF) purification as described previously, to yield a 4 layered siRNA containing NP (Figure 1A). HA binds the CD44 receptor,(Zhou J Deng et al., 2013; Gu et al., 2017) which is overexpressed in several aggressive solid epithelial cancers, including many forms of non-small cell lung cancer, advanced serous ovarian cancer, triple negative breast cancer, and other tumorigenic cells.(Zhou J Deng et al., 2013; Gu et al., 2017) The resulting nanoparticles display a strong negative surface charge and a high degree of hydration that limits non-specific interactions with cells, while promoting CD44-specific tumor cell uptake. (Zhou J Deng et al., 2013)

Comparison of electron micrographs of the MSNs that act as cores for electrostatic assembly (Figure1B) and the LbL nanoparticles formed from the MSN cores (Figure 1C) indicated an ultrathin outer particle polyelectrolyte complex shell of low electron density, characteristic of LbL nanoparticles.

Deposition of PLR (layer no.1) onto MSNs (denoted as layer no.0) was corroborated by DLS measurements indicating an increase in hydrodynamic size, as well as in the complete reversal of surface charge (Figure 1D,E). The addition of subsequent layers consisting of siRNA (layer no.2), PLR (layer no.3), and HA (layer no.4), respectively, also increased particle size (approximately 32.2 nm for the first layer of PLR, 3.43 nm for siRNA, 5.6 nm for the second layer of PLR, and 42.4 nm for the HA layer) provides a high level of surface hydration to the particles, contributing to the nanoparticles' steric stability.(Dreaden et al., 2015) Also, this final HA layer is thought to be highly hydrated thus yielding a thicker, but possible higher water content outer layer, when measured hydrodynamically.(Gu et al.,

2017) The uniformity of the layer deposition was evidenced by the conservation of the polydispersity following each layer, as depicted in Figure 1F.

The amount of siRNA in the LbL nanosystems was investigated immediately after siRNA layer deposition, also using the progressive enzymatic degradation of the deposited layers on the final LbL nanoconstruct.(Okuda et al., 2013),(Choi et al., 2010),(Zeng et al., 2004) Ribogreen quantification took place again, and the amount AF 488 siRNA was also measured. The amount of total siRNA is displayed in Table 1. An agarose gel electrophoresis (Figure S1) evaluated siRNA integrity. To that end, heparin, generally used to unpack nucleic acids from nucleic acid/cationic vectors,(Okuda et al., 2013) enabled the detection of the electrophoretic band of siRNA.

Since particle size and shape are both critical to powder inhalation, LbL nanoparticles were micronized via inclusion into CHT dry powders to optimize aerodynamic performance. Thus, CHT, CHT-MSN and CHT-LbL siRNA powders were produced by supercritical CO_2-assisted spray drying (SASD), a green process based on the solubilization of controlled quantities of CO_2 into the liquid solution. In fact, SADS technology has been widely explored as an efficient, versatile, potentially continuous and scalable technique for the preparation of nano- and microparticles with suitable properties for pulmonary administration, and has been further optimized by the group.(Aguiar-Ricardo and Costa, 2019; Cabral et al., 2016) However, due to the typical lack of total efficiency of a cyclone operating in a small scale operation, smaller particles may have escaped through the gas stream.(Costa et al., 2018) The entrapment efficiency of the LbL nanoparticles (28.7%) in the CHT powder was assessed by measuring the fluorescence of IR-780 dye present in the microspheres. Due to process limitations, CHT-LbL siRNA powders were produced by combining proportionally both siRNA LbL nanoparticles (KRAS 1211 modified siRNA and NC siRNA) in order to enhance the amount of fluorescent siRNA (present in both nanoformulations) for a more accurate biodistribution panel. The limited entrapment efficiency obtained with this small-scale apparatus is expected to be improved at an industrial scale. Further measurements appear in Table 2.

The final formulations (CHT, CHT-MSN, CHT-LbL siRNA) showed no significant difference in their volume mean diameters ($D_{v,50}$), which ranged from 3 to 4 μm, the ideal particle size for pulmonary inhalation.(Okuda et al., 2013) Similar relative width of the distribution (span) values was obtained for all types of CHT microparticles, indicating that these have the same distribution width (Table S1).

The Karl Fisher assay showed that lower moisture contents were found each time.(Cabral et al., 2016; Restani et al., 2016; A. S. Silva et al., 2017) Although the differences among the obtained values were not statistically significant, moisture percentages appeared to decrease with nanoparticle addition.

The X-ray diffraction (XRD) patterns of MSN and CHT and CHT-MSN samples are displayed Figure S2. Due to the amount of sample required to perform XRD analysis, the sample CHT-LbL siRNA was not investigated using this technique. However, the pattern is expected to be very similar to that for CHT-MSN. The characteristic spectra and peak of

amorphous SiO_2 was depicted at 2 = 20° for MSN. Similarly, the characteristic pattern of processed CHT also showed a broadening at 2 = 20° of a type also depicted for CHT-MSN powders. The powders' surface areas (displayed in Table S1) exhibited values ranging from 7.1 (CHT) and 6.3 m^2/g (CHT-MSN) and, consistent with pore classification adopted by IUPAC,(Bering et al., 1966) both types of particles presented mesopores (1.5 nm < d < 50 nm). Moreover, the analysis of BET isotherms (Figure S3) showed that the microparticles followed a Type II isotherm, common for multilayer absorptions,(Rouquerol et al., 1999) indicating the formation of an adsorbed layer whose thickness increased with relative pressure until it equaled saturation vapor pressure, at which point the adsorbed layer became a bulk liquid. The uptake at *Point I* (Figure S3) represented the completion of the monolayer and estimated how much adsorbate was required to form a monolayer covering the solid surface. At this point a quasilinear section emerged, representing the formation of the multilayer.(Kean and Thanou, 2010) The relatively small surface area values also indicated a more energetically favorable state.(Vehring, 2008) Figure1G and H display the SEM micrographs of CHT particles and CHT-LbL siRNA powders, respectively, demonstrating smooth to rough spherical particles in both formulations. STEM images and EDX analysis of such samples are displayed Figure S4. To further investigate nanoparticle localization inside the microparticles, the microspheres were observed using CLSM and a 3D reconstruction was performed with the aid of Imaris Bitplane. All of the microspheres were placed on glass-bottomed coverslips containing culture media, after which the particles were immediately observed. The resulting images are depicted in Figure 1J and K. CHT autofluorescence allowed for the visualization of the particle matrix. AF 488 siRNA can be seen in green, representing nanoparticle location within the microparticle. Nanoparticles appeared to be located in the outermost regions (Figure 1J), corroborating the results obtained by STEM and EDX conjugation (Figure S4). Upon a transversal cut, the blue color, corresponding to CHT autofluorescence, seems to be increasingly located inside the formed microparticle. However, the presence of siRNA LbL nanoparticles can be also identified inside the particle, as a mix of the blue and green (Figure 1K). Key literature mentions no consensual procedures for describing particle formation, but there are general tendencies that can be used to explain the process. The shriveling seen in SEM images result from high solvent evaporation rate over the diffusion coefficient of the solute. When the ratio of evaporation rate over diffusion rate increases, the higher molecular weight polymer tends to accumulate at the surface, forming a shell that may then deform in various ways.(Moura et al., 2014; Vehring, 2008) As the suspended nanoparticles have also low mobility, with increasing concentration upon solvent and co-solvent evaporation, they start to form a composite shell and phase separate throughout the bulk of the droplet. Factors governing particle formation, such as air temperature, which aids particle drying as well as the EtOH percentage, may contribute to rapid solvent evaporation. On the other hand, silica has also been described as a drying auxiliary agent and a CO_2 absorbent.(Wang et al., 2014) Its very low moisture content also corroborates an efficient drying process.

The powder aerosolization characteristics of CHT-MSN and CHT were assessed *in vitro* using a dry powder breath activated inhaler device (Aerolizer™) with the aid of an Anderson Cascade Impactor (ACI). The percentage of powder deposited at each stage of the ACI, inhaler, capsule, and induction port, was calculated gravimetrically and is plotted on Figure

1I. The Cascade Impactor measurements are depicted in Table S2. The emitted dose (ED %), equal to the amount of powder fluidized through the inhaler, varied between 70.2 % and 75.2 %. It was also found that, for these formulations, the fine particle fraction (FPF %), i.e. the respirable fraction most likely to be deposited in the deep lung, was 54.3 % to CHT and 44.4 % for the CHT-MSN formulation, nearly matching the dry powder inhalers (DPIs) currently available on the market.(El-Sherbiny and Smyth, 2010; Silva et al., 2014b) Figure 1I shows that a significant percentage of powder weight was lost in the inhaler and induction port, which simulates the upper airways. This may be explained by the formation of turbulent eddies in this area, humidity, chitosan mucoadhesive properties or the electrostatic energy of the powders. Although there was a slight difference between the values, no significant difference between CHT and CHT-MSN powders in the same stage of the ACI was identified. However, due to the greater surface irregularity of CHT microparticles, we had already predicted an enhanced flowability of this particular type of particle.

3.2. *In vitro* performance of the LbL nanoparticles and their micronized formulations

The *in vitro* siRNA release (in PBS) from the LbL nanoconstructs at different pH values is displayed in Figure 2A, suggesting a controlled and sustained release of the siRNA from the nanoassemblies over an extended period of time. After 72 h at pH 5.5 (which mimics the endosomal/lysosomal pH)(Xu et al., 2015b, 2015a), the release was slightly higher than that at pH 6.8 (extracellular pH of tumor niche)(Caruso et al., 2012; Webb et al., 2011) and 7.4 (physiological pH), releasing 15% of the loaded siRNA. The gathered data suggest that the amount of encapsulated siRNA was not completely released after 72 h, as demonstrated by the slope of the release curves between the 50-72 hours, being more pronounced at the solution pH 5.5. We also looked at the cytotoxicity profile of the nanocarriers. Figure 2C demonstrates little observable cytotoxicity by these LbL assemblies.

The siRNA delivery by aerosolized LbL was investigated in tdTomato–expressing KP cells (these cells are lung cancer cells that are derived from tumors of a NSCLC autochthonous model with adenovirus-induced expression of KrasG12D and homozygous p53 targeting) (Chung et al., 2017) (Figure 2B). LbL nanoparticles containing KRAS 1211 modified siRNA achieved 50% gene silencing (either 10-100 nM siRNA) versus untreated cells as a control. Cellular internalization of MSN LbL NPs was demonstrated in this case by FACS and confocal laser scanning microscopy (CLSM, (Figure 2D, E and F, respectively)).

The cumulative release profiles of the LbL siRNA nanoparticles and the siRNA from the microparticles at pHs 7.4 and 6.8 are depicted in Figure 3A. For these *in vitro* studies, only the CHT-LbL siRNA formulation was assessed. To evaluate the release of nanoparticles from the microparticles, IR-780 dye fluorescence was monitored at pre-determined end points (Figure 3A). A Ribogreen assay quantified the amount of siRNA released along the same end points (Figure 3B). After 120h, 10.2% to 13.6% (pH 7.4 and pH 6.8, respectively) of the siRNA was released from the microparticles. Since Ribogreen measures the total siRNA in the sample and not the amount of dissociated/released siRNA, the measured siRNA may still be encapsulated within the LbL NPs in these measurements. Likewise, according to the IR-780 dye intensity, the quantity of nanoparticles released from the micropowders varied from 72 to 80 % for pH 7.4 and 6.8, respectively. Since CHT pKa was

6.5, it is to be expected that CHT amino groups would be partially protonated at pH 6.8, leading to easier powder dissolution and, consequently, faster release. The diffusion mechanism of the LbL nanosystems and siRNA through the microparticles was evaluated by fitting the obtained data with the Korsmeyer and Peppas equation (Figure S5). Based on the diffusion exponent (n) of both systems in both pHs (between 0.38 and 0.44), their release profile from the microspheres took place via Fickian diffusion.(Siepmann and Siepmann, 2008) The presence of pores on the particles' surface allowing for superficial retention of nanoparticles may have contributed to the sustained and controlled release observed at the end of the experiment. The percentage of the aerosolized powders (CHT and CHT-MSN) that was eventually able to reach the deep lung, FPF%, is depicted in Figure 3C.

The ability of the CHT-LbL siRNA powders to silence KRAS genes was investigated in tdTomato–expressing KP cells and appears in Figure 3D. Increased concentrations of particles and, consequently, KRAS siRNA, were investigated. Gene expression of treated cells was compared to that of untreated ones. CHT-LbL siRNA microparticles were found to be able to achieve over 90 % gene silencing (for both 25 and 100 ng of siRNA KRAS), which is greater than the 50% silencing observed with just the LbL nanoparticles alone, (for both 26 and 260 ng of siRNA KRAS). We hypothesize that this increase in treatment efficacy, when compared to the nanoparticles, can be attributed to the presence of some free CHT polymer chains that may be taken up by cells along with our nanovehicles. Briefly, after endocytosis, CHT can trigger an increased osmotic pressure. In fact, CHT protonation inside the endosomes (CHT pka ≈ 6.5 and endosomal pH ≈ 6.5) will cause chlorine ion influx and consequently, protons and water causing an endosomal burst, releasing its content to the cytosol. Afterwards, the siRNA released from the LbL nanoparticle can be released from the endosome into the cytosol, where it can bind to RNA-induced silencing complex (RISC) and enact gene silencing. Since both KRAS and NC siRNA nanoparticles were conjugated in order to produce the micronized powders, only half of the siRNA entrapped per gram of powder corresponded to LbL KRAS siRNA nanoparticles (the other half is representative of the LbL NC siRNA nanoparticles), whose KRAS siRNA is 89.3% (based on Table 1). It was, therefore, possible to estimate (based on the E% on Table 2) that 120 μg of micronized powder contained approximately 100 ng of KRAS siRNA, whereas 30 μg have 25 ng of siRNA KRAS.

Cell viability of the micronized powders was also addressed. As Figure 3E shows, cytotoxicity is low, as demonstrated by the micronized powders, whose cell viability is always above 80 %. Slight variations were observed. However, there was no significant statistical difference between the negative control (cells) and the incubated ones. Powder interactions with cells were also investigated after 1 and 12 h using CSLM and their images appear in Figure 3F and G. After 1 h of incubation, green puncta from AF 488 siRNA can be identified among the cellular environment (Figure 3F). After 12 h of incubation, the siRNA from the CHT microparticles was even more evident and concentrated within the cytosol, as demonstrated in Figure 3G. These results agreed with the release profile of both the LbL nanosystems as well as the labeled siRNA from the microspheres. It is also worth pointing out that microparticle adhesion to cells may be attributed to the outermost location of the LbL nanoparticles. In fact, since HA was the last layer in our LbL assembly, its interaction

with CD44 receptors in tdTomato expressing KP cell line(Gu et al., 2017) governed the higher levels of binding and internalization observed.

3.3. *In vivo* preliminary biodistribution of the CHT-LbL siRNA powder

Although some literature reports already demonstrated the administration of siRNA through the inhalation route,(Agnoletti et al., 2017; Chow et al., 2017; De Backer et al., 2015; Okuda et al., 2018, 2013; Sharma et al., 2013; Xu et al., 2018; Youngren-ortiz et al., 2017) the pulmonary delivery of micronized siRNA through the SADS technology has, for the best of our knowledge, never been attempted. Hence, to investigate the ability of the formulated powders as future vehicles for therapeutic siRNA delivery via the pulmonary route, we have performed a preliminary and proof-of-concept study in which the microencapsulated LbL siRNA nanovehicles were administered following pulmonary delivery in healthy female BALB/c mice. Unloaded CHT microparticles (no LbL nanosystems incorporated) were used as a control. Mice treated with CHT-LbL siRNA microparticles were imaged using an IVIS imaging system after 30 min and 24 h (Figure 4A). CHT microparticle autofluorescence also appears in IVIS imaging. (Figure 4B). In all three groups, fluorescent signal could be observed in the lobes of the lungs, showing that the aerosol could indeed reach the deep lung area. The excised lungs were scanned using two imaging techniques: two photon correlation microscopy (TPCM) and CLSM, as shown in Figure 4C and D (respectively). Both methods showed a higher fluorescence intensity in the green channel for samples containing CHT-LbL siRNA. From the TPCM images, particle density appeared to be higher at 24 h (Figure 4C-2) than at 30 min (Figure 4C-1), contradicting the results from the IVIS epi-fluorescence measurement. Dry powders (microspheres) seemed to deposit deeply within the alveolar region (better regional distribution), as they exhibited adequate aerodynamic properties.

Histopathologic analyses of the mice's lungs evaluated the impact of the micropowders on lung tissue. The lungs of mice receiving blank CHT microparticles and untreated ones were used as controls. Lung section histology analyses are displayed in Figure 4E-F. Unstained sections were imaged using TPCM (Figure 4E) and sections stained with Hematoxylin and Eosin (H&E) were analyzed using a Nikon light microscope (Figure 4F). Figure 4E revealed the presence of microparticles mainly portrayed in CHT-LbL siRNA 30 min and 24 hours (depicted in green, Figure 4E-1 and 2). H&E staining (Figure 4F) revealed the presence of enhanced blue/purple coloration (hematoxylin staining) in all treated lungs. We anticipate the local inflammation observed at 24 hours to be transient, but further studies will be required to exhaustively characterize the biocompatibility of this platform. However, prior research has demonstrated that the administration of CHT and other polymeric particles to the lungs have revealed low lung toxicity following bronchoalveolar lavage fluid.(Al-Qadi et al., 2012; Ortiz et al., 2015; Pai et al., 2015; Qu et al., 2017) Visual microscopic comparison between untreated and treated lungs, showed that neither structural rupture nor septal thickness were evidenced in the treated lungs.

In addition, serum biochemistry analyses were also recovered at the end of the experiment (24 h) (Figure S6). The results were compared to the dynamic reference range of the assay given by Charles River laboratories, and showed no sign of liver or kidney damage,

suggesting that the micronized powders and the LbL nanosystems exhibited little serum toxicity at the administered dose.

This preliminary data demonstrates the ability of the DPIs engineered through the SASD technology in reaching the deep lung regions. Although this is a quite promising outcome, further possible adverse effects should be tested, by measuring specific biomarkers in the lungs such as lactate dehydrogenase leakage and inflammatory cytokine concentration in bronchoalveolar lavage fluid. In addition, since the *in vivo* study only aimed to investigate the ability to deliver this newly engineered powders directly to the lungs and its deposition in the alveolar area, no further *in vivo* gene silencing was addressed. Therefore, for therapeutic validation, forthcoming studies should focus on the ability to *in vivo* knock-down KRAS in clinically relevant models. As cell viability is not strongly impaired in this study, further conjugation with therapeutic agents specific to the molecular profile of the tumor can be later conjugated with this new platform in order to increase the effectiveness of the treatment.

Taken together, the results suggest that the encapsulation of the siRNA-assembled LbL nanoparticles using SASD technology, enabled the fabrication of powders with characteristics matching those encountered in the market for administration using DPI, (El-Sherbiny and Smyth, 2010; Silva et al., 2014b) with satisfactory *in vitro* results.

4. Conclusions

In the present study, LbL nanosystems comprising a nanolayer of KRAS siRNA were successfully engineered. The developed LbL assemblies achieved significant impact on the reduction of KRAS gene expression *in vitro*. Micronization of these nanoparticles into CHT powders using the green SASD technology enabled the design and production of effective systems for pulmonary delivery of siRNA. The ability of the micronized siRNA to reduce KRAS gene expression *in vitro* revealed nucleic acid stability even after powder production. Moreover, the controlled and sustained release for each assembled nanosystem and siRNA proved that our micronized systems are suitable for a controlled pulmonary delivery. *In vivo* preliminary biodistribution assessment of the micro formulations in healthy mice showed deep lung diffusion and an alveolar distribution of the powders. In summary, the results suggest a potential strategy for delivering siRNA to the lungs for the treatment of lung adenocarcinoma. The presence of the IR-780 dye onto the MSN core of the LbL nanoassemblies further enhances the potential to combine therapeutic approaches, such as photothermal therapy (PTT) with gene therapy, potentially increasing lung cancer regression.

Supplementary Material

Refer to Web version on PubMed Central for supplementary material.

Acknowledgments

We are grateful for the financial support of the Associate Laboratory for Green Chemistry LAQV-REQUIMTE, which is financed by national funds from FCT/MCTES (UID/QUI/50006/2019) and co-financed by the ERDF under the PT2020 Partnership Agreement (POCI-01-0145-FEDER-007265). This work was supported by the US

Department of Defense Congressionally Directed Medical Research Programs (PTH, Teal Innovator Award 13-1-0151), the Ovarian Cancer Research Fund (PTH, Collaborative Research Development Grant), the National Institutes of Health (ECD, NIBIB 1F32EB017614), and the National Science Foundation (SC, GFRP 1122374). Resources were provided in part by the Koch Institute Support Grant (P30-CA14051) from the National Cancer Institute and the MIT MRSEC Shared Experimental Facilities Grant (DMR-0819762) from the National Science Foundation. We thank the Koch Institute Swanson Biotechnology Center for technical support, including the flow cytometry, Peterson nanotechnology, microscopy, ATWAI, and Tang Histology facilities. We also wish to thank our fellow lab members for helpful discussions. We also acknowledge PhD grants SFRH/BD/51584/2011 (A. Sofia Silva) and one FCT-Lisbon for the IF/00915/2014 contract (T. Casimiro). The MIT-Portugal Program (Bioengineering Systems Focus Area) also merits our gratitude.

References

Agnoletti M, Bohr A, Thanki K, Wan F, Zeng X, Boetker JP, Yang M, Foged C, 2017. Inhalable siRNA-loaded nano-embedded microparticles engineered using microfluidics and spray drying. Eur. J. Pharm. Biopharm 120, 9–21. 10.1016/j.ejpb.2017.08.001 [PubMed: 28780275]

Aguiar-Ricardo A, Costa E, 2019. Supercritical Fluid Manufacture, in: Hickey AJ, da Rocha SRP (Eds.), Pharmaceutical Inhalation Aerosol Technology, Third Edition. CRC Press.

Al-Qadi S, Grenha A, Carrión Recio D, Seijo B, Remuñán-López C, 2012. Microencapsulated chitosan nanoparticles for pulmonary protein delivery: in vivo evaluation of insulin-loaded formulations. J. Control. Release 157, 383–390. 10.1016/j.jconrel.2011.08.008 [PubMed: 21864592]

Amidi M, Pellikaan HC, de Boer AH, Crommelin D.J. a, Hennink WE, Jiskoot W, 2008. Preparation and physicochemical characterization of supercritically dried insulin-loaded microparticles for pulmonary delivery. Eur. J. Pharm. Biopharm 68, 191–200. 10.1016/j.ejpb.2007.05.007 [PubMed: 17576056]

Bering BP, Dubinin MM, Serpinsky VV, 1966. Theory of volume filling for vapor adsorption. J. Colloid Interface Sci 21, 378–393. 10.1016/0095-8522(66)90004-3

Cabral RP, Sousa AML, Silva AS, Paninho AI, Temtem M, Costa E, Casimiro T, Aguiar-Ricardo A, 2016. Design of experiments approach on the preparation of dry inhaler chitosan composite formulations by supercritical CO 2 -assisted. J. Supercrit. Fluids 116, 26–35. 10.1016/j.supflu.2016.04.001

Caruso F, Hyeon T, Rotello V, Lee D, Koo H, Sun I, Ryu JH, Kim K, Kwon IC, 2012. Nanomedicine themed issue Multifunctional nanoparticles for multimodal imaging and theragnosis w. Chem. Soc. Rev 41, 2656–2672. 10.1039/c2cs15261d [PubMed: 22189429]

Choi KY, Chung H, Min KH, Yoon HY, Kim K, Park JH, Kwon IC, Jeong SY, 2010. Self-assembled hyaluronic acid nanoparticles for active tumor targeting. Biomaterials 31, 106–114. 10.1016/j.biomaterials.2009.09.030 [PubMed: 19783037]

Chow MYT, Qiu Y, Lo FFK, Lin HHS, Chan HK, Kwok PCL, Lam JKW, 2017. Inhaled powder formulation of naked siRNA using spray drying technology with L-leucine as dispersion enhancer. Int. J. Pharm 530, 40–52. 10.1016/j.ijpharm.2017.07.013 [PubMed: 28720537]

Chung W-J, Daemen A, Cheng JH, Long JE, Cooper JE, Wang B, Tran C, Singh M, Gnad F, Modrusan Z, Foreman O, Junttila MR, 2017. Kras mutant genetically engineered mouse models of human cancers are genomically heterogeneous. Proc. Natl. Acad. Sci 114, E10947–E10955. 10.1073/pnas.1708391114 [PubMed: 29203670]

Conde J, Ambrosone A, Hernandez Y, Tian F, McCully M, Berry CC, Baptista PV, Tortiglione C, de la Fuente JM, 2015. 15 years on siRNA delivery: Beyond the State-of-the-Art on inorganic nanoparticles for RNAi therapeutics. Nano Today 10, 421–450. 10.1016/j.nantod.2015.06.008

Connor EE, Mwamuka J, Gole A, Murphy CJ, Wyatt MD, 2005. Gold nanoparticles are taken up by human cells but do not cause acute cytotoxicity. Small 1, 325–327. 10.1002/smll.200400093 [PubMed: 17193451]

Correa S, Choi KY, Dreaden EC, Renggli K, Shi A, Gu L, Shopsowitz KE, Quadir MA, Ben-Akiva E, Hammond PT, 2016. Highly Scalable, Closed-Loop Synthesis of Drug-Loaded, Layer-by-Layer Nanoparticles. Adv. Funct. Mater 26, 991–1003. 10.1002/adfm.201504385 [PubMed: 27134622]

Correa S, Dreaden EC, Gu L, Hammond PT, 2015. Engineering nanolayered particles for modular drug delivery. J. Control. Release 240, 364–386. 10.1016/j.jconrel.2016.01.040

Costa C, Casimiro T, Aguiar-Ricardo A, 2018. Optimization of Supercritical CO 2 -Assisted Atomization: Phase Behavior and Design of Experiments. J. Chem. Eng. Data 63, 885–896. 10.1021/acs.jced.7b00820

Council of Europe, 2010. Preparations for Inhalation: Aerodynaminc Assessment of Fine Particles, in: European Pharmacopeia. pp. 274–285.

De Backer L, Cerrada A, Pérez-Gil J, De Smedt SC, Raemdonck K, 2015. Bio-inspired materials in drug delivery: Exploring the role of pulmonary surfactant in siRNA inhalation therapy. J. Control. Release 220, 642–650. 10.1016/j.jconrel.2015.09.004 [PubMed: 26363301]

Deng, Zhou J, Morton SW, Ben-akiva E, Dreaden EC, Shopsowitz KE, Hammond PT, 2013. Layer-by-Layer Nanoparticles for Systemic Codelivery of an Anticancer Drug and siRNA for Potential Triple-Negative Breast Cancer Treatment. ACS Nano 7, 9571–9584. [PubMed: 24144228]

Deng, Zhou J, Morton SW, Ben-Akiva E, Dreaden EC, Shopsowitz KE, Hammond PT, 2013. Layer-by-layer nanoparticles for systemic codelivery of an anticancer drug and siRNA for potential triple-negative breast cancer treatment. ACS Nano 7, 9571–9584. 10.1021/nn4047925 [PubMed: 24144228]

Domínguez-delgado CL, Rodríguez-cruz IM, Fuentes-prado E, Escobar-chávez JJ, Vidal-romero G, García-gonzález L, Puente-lee RI, 2014. Drug Carrier Systems Using Chitosan for Non Parenteral Routes, in: Gowder SJT (Ed.), Pharmacology and Therapeutics. InTech, pp. 273–275.

Dreaden EC, Morton SW, Shopsowitz KE, Choi J, Deng ZJ, 2015. Bimodal Tumor-Targeting from Microenvironment Responsive. ACS Nano 8, 8374–8382.

Dufort S, Bianchi A, Henry M, Lux F, Le Duc G, Josserand V, Louis C, Perriat P, Crémillieux Y, Tillement O, Coll J-L, 2015. Nebulized Gadolinium-Based Nanoparticles: A Theranostic Approach for Lung Tumor Imaging and Radiosensitization. Small 11, 215–221. 10.1002/smll.201401284 [PubMed: 25201285]

El-Sherbiny IM, Smyth HDC, 2010. Biodegradable nano-micro carrier systems for sustained pulmonary drug delivery: (I) self-assembled nanoparticles encapsulated in respirable/swellable semi-IPN microspheres. Int. J. Pharm 395, 132–141. 10.1016/j.ijpharm.2010.05.032 [PubMed: 20580794]

FDA approves first-of-its kind targeted RNA-based therapy to treat a rare disease [WWW Document], 2018. URL https://www.fda.gov/newsevents/newsroom/pressannouncements/ucm616518.htm (accessed 10.22.18).

Feldmann DP, Merkel OM, 2015. The advantages of pulmonary delivery of therapeutic siRNA. Ther. Deliv 6, 1239–1241. 10.1002/9781118903681 [PubMed: 26584253]

Grenha A, Al-Qadi S, Seijo B, Remuñán-López C, 2010. The potential of chitosan for pulmonary drug delivery. J. Drug Deliv. Sci. Technol 20, 33–43. 10.1016/S1773-2247(10)50004-2

Gu L, Deng ZJ, Roy S, Hammond PT, 2017. A combination RNAi-chemotherapy layer-by-layer nanoparticle for systemic targeting of KRAS/P53 with cisplatin to treat non–small cell lung cancer. Clin. Cancer Res 23, 7312–7323. 10.1158/1078-0432.CCR-16-2186 [PubMed: 28912139]

Hartmann H, Hossfeld S, Schlosshauer B, Mittnacht U, Pêgo AP, Dauner M, Doser M, Stoll D, Krastev R, 2013. Hyaluronic acid / chitosan multilayer coatings on neuronal implants for localized delivery of siRNA nanoplexes. J. Control. Release 168, 289–297. 10.1016/j.jconrel.2013.03.026 [PubMed: 23562632]

Jae HP, Kwon S, Lee M, Chung H, Kim JH, Kim YS, Park RW, Kim IS, Sang BS, Kwon IC, Seo YJ, 2006. Self-assembled nanoparticles based on glycol chitosan bearing hydrophobic moieties as carriers for doxorubicin: In vivo biodistribution and anti-tumor activity. Biomaterials 27, 119–126. 10.1016/j.biomaterials.2005.05.028 [PubMed: 16023198]

Jere D, Jiang HL, Kim YK, Arote R, Choi YJ, Yun CH, Cho MH, Cho CS, 2009. Chitosan-graft-polyethylenimine for Akt1 siRNA delivery to lung cancer cells. Int. J. Pharm 378, 194–200. 10.1016/j.ijpharm.2009.05.046 [PubMed: 19501140]

Kean T, Thanou M, 2010. Biodegradation, biodistribution and toxicity of chitosan. Adv. Drug Deliv. Rev 62, 3–11. 10.1016/j.addr.2009.09.004 [PubMed: 19800377]

Krieg B, Hirsch M, Scholz E, Nuhn L, Tabujew I, Bauer H, Decker S, Khobta A, Schmidt M, Tremel W, Zentel R, Peneva K, Koynov K, Mason a. J., Helm M, 2014. New Techniques to Assess In

Vitro Release of siRNA from Nanoscale Polyplexes. Pharm. Res 32, 1957–1974. 10.1007/s11095-014-1589-7 [PubMed: 25488263]

Lam JKW, Liang W, Chan HK, 2012. Pulmonary delivery of therapeutic siRNA. Adv. Drug Deliv. Rev 64, 1–15. 10.1016/j.addr.2011.02.006 [PubMed: 21356260]

Maggini L, Cabrera I, Ruiz-Carretero A, Prasetyanto EA, Robinet E, De Cola L, 2016. Breakable mesoporous silica nanoparticles for targeted drug delivery. Nanoscale 8, 7240–7247. 10.1039/C5NR09112H [PubMed: 26974603]

Malmsten M, 2013. Inorganic nanomaterials as delivery systems for proteins, peptides, DNA, and siRNA. Curr. Opin. Colloid Interface Sci 18, 468–480. 10.1016/j.cocis.2013.06.002

Merkel OM, Rubinstein I, Kissel T, 2014. siRNA Delivery to the lung: What's new? Adv. Drug Deliv. Rev 75, 112–128. 10.1016/j.addr.2014.05.018 [PubMed: 24907426]

Moreira AF, Gaspar VM, Costa EC, de Melo-Diogo D, Machado P, Paquete CM, Correia IJ, 2014. Preparation of end-capped pH-sensitive mesoporous silica nanocarriers for on-demand drug delivery. Eur. J. Pharm. Biopharm 88, 1012–1025. 10.1016/j.ejpb.2014.09.002 [PubMed: 25229810]

Morrison C, 2018. Alnylam prepares to land first RNAi drug approval. Nat. Rev. Drug Discov 17, 156–157. 10.1038/nrd.2018.20 [PubMed: 29487392]

Moura C, Neves F, Costa E, 2014. Design of Composite Particles via Spray Drying for DPI Formulations. ONdrugDelivery 53, 16–23.

Naikwade SR, Bajaj AN, Gurav P, Gatne MM, Singh Soni P, 2009. Development of budesonide microparticles using spray-drying technology for pulmonary administration: design, characterization, in vitro evaluation, and in vivo efficacy study. AAPS PharmSciTech 10, 993–1012. 10.1208/s12249-009-9290-6 [PubMed: 19649711]

Okuda T, Kito D, Oiwa A, Fukushima M, Hira D, Okamoto H, 2013. Gene silencing in a mouse lung metastasis model by an inhalable dry small interfering RNA powder prepared using the supercritical carbon dioxide technique. Biol. Pharm. Bull 36, 1183–1191. [PubMed: 23811567]

Okuda T, Morishita M, Mizutani K, Shibayama A, Okazaki M, Okamoto H, 2018. Development of spray-freeze-dried siRNA/PEI powder for inhalation with high aerosol performance and strong pulmonary gene silencing activity. J. Control. Release 279, 99–113. 10.1016/j.jconrel.2018.04.003 [PubMed: 29627404]

Ortiz M, Jornada DS, Pohlmann AR, Guterres SS, 2015. Development of Novel Chitosan Microcapsules for Pulmonary Delivery of Dapsone : Characterization , Aerosol Performance , and In Vivo Toxicity Evaluation. J. Aerosol Med. Pulm. Drug Deliv 16, 18–20. 10.1208/s12249-015-0283-3

Pai RV, Jain RR, Bannalikar AS, Menon MD, 2015. Preparation and Evaluation of Surface Modified Lactose Particles for Improved Performance of Fluticasone Propionate Dry Powder Inhaler. J. Aerosol Med. Pulm. Drug Deliv 28, 1–17. 10.1089/jamp.2014.1187 [PubMed: 24914770]

Qu S, Zhao L, Zhu J, Wang C, Dai C, Guo H, Qu S, Zhao L, Zhu J, Wang C, Dai C, Guo H, Hao Z, 2017. Preparation and testing of cefquinome-loaded poly lactic-co-glycolic acid microspheres for lung targeting Preparation and testing of cefquinome-loaded poly lactic-co-glycolic. Drug Deliv. 24, 745–751. 10.1080/10717544.2017.1321058 [PubMed: 28454494]

Restani RB, Silva AS, Pires RF, Cabral RP, Correia IJ, Casimiro T, Bonifácio VDB, Aguiar-Ricardo A, 2016. Nano-in-Micro POxylated Polyurea Dendrimers and Chitosan Dry Powder Formulations for Pulmonary Delivery. Part. Part. Syst. Charact 33, 851–858.

Ritger PL, Peppas N. a., 1987. A simple equation for description of solute release I. Fickian and non-fickian release from non-swellable devices in the form of slabs, spheres, cylinders or discs. J. Control. Release 5, 23–36. 10.1016/0168-3659(87)90034-4

Rouquerol F, Rouquerol J, Sing KSW, 1999. Interpretation of Physisorption Isotherms at the Gas-Solid Interface, in: Rouquerol F, Rouquerol J, Sing KSW (Eds.), Adsorption by Powders and Porous Solids. Academic Press, San Diego, pp. 93–115. 10.1016/B978-012598920-6/50005-1

Sharma K, Somavarapu S, Colombani A, Govind N, Taylor KMG, 2013. Nebulised siRNA encapsulated crosslinked chitosan nanoparticles for pulmonary delivery. Int. J. Pharm 455, 241–247. 10.1016/j.ijpharm.2013.07.024 [PubMed: 23876499]

Siepmann J, Siepmann F, 2008. Mathematical modeling of drug delivery. Int. J. Pharm 364, 328–343. 10.1016/j.ijpharm.2008.09.004 [PubMed: 18822362]

Silva AS, Sousa AM, Cabral RP, Silva MC, Costa C, Miguel SP, Bonifácio VDB, Casimiro T, Correia IJ, Aguiar-Ricardo A, 2017. Aerosolizable gold nano-in-micro dry powder formulations for theragnosis and lung delivery. Int. J. Pharm 519, 240–249. 10.1016/j.ijpharm.2017.01.032 [PubMed: 28111281]

Silva AS, Tavares MT, Aguiar-Ricardo A, 2014a. Sustainable strategies for nano-in-micro particle engineering for pulmonary delivery. J. Nanoparticle Res 16, 2602–2619. 10.1007/s11051-014-2602-0

Silva AS, Tavares MT, Aguiar-Ricardo A, 2014b. Sustainable strategies for nano-in-micro particle engineering for pulmonary delivery. J. Nanoparticle Res 16, 2602–2619. 10.1007/s11051-014-2602-0

Silva MC, Silva AS, Fernandez-Lodeiro J, Casimiro T, Lodeiro C, Aguiar-Ricardo A, 2017. Supercritical CO2-assisted spray drying of strawberry-like gold-coated magnetite nanocomposites in chitosan powders for inhalation. Materials (Basel). 10, 74–89. 10.3390/ma10010074

Taratula O, Garbuzenko OB, Chen AM, Minko T, 2011. Innovative strategy for treatment of lung cancer: targeted nanotechnology-based inhalation co-delivery of anticancer drugs and siRNA. J. Drug Target 19, 900–914. 10.3109/1061186X.2011.622404 [PubMed: 21981718]

Tavares M, Cabral RP, Costa C, Martins P, Fernandes AR, Casimiro T, Aguiar-Ricardo A, 2017. Development of PLGA dry powder microparticles by supercritical CO2-assisted spray-drying for potential vaccine delivery to the lungs. J. Supercrit. Fluids 128, 235–243. 10.1016/j.supflu.2017.06.004

Temtem M, Barroso T, Casimiro T, Mano JF, Aguiar-Ricardo A, 2012. Dual stimuli responsive poly(N-isopropylacrylamide) coated chitosan scaffolds for controlled release prepared from a non residue technology. J. Supercrit. Fluids 66, 398–404. 10.1016/j.supflu.2011.10.015

The top 10 causes of death [WWW Document], 2018. URL http://www.who.int/news-room/fact-sheets/detail/the-top-10-causes-of-death (accessed 10.15.18).

Vehring R, 2008. Pharmaceutical particle engineering via spray drying. Pharm. Res 25, 999–1022. 10.1007/s11095-007-9475-1 [PubMed: 18040761]

Wang J, Huang L, Yang R, Zhang Z, Wu J, Gao Y, Wang Q, O'Hare D, Zhong Z, 2014. Recent advances in solid sorbents for CO_2 capture and new development trends. Energy Environ. Sci 7, 3478–3518. 10.1039/C4EE01647E

Webb BA, Chimenti M, Jacobson MP, Barber DL, 2011. Dysregulated pH: A perfect storm for cancer progression. Nat. Rev. Cancer 11, 671–677. 10.1038/nrc3110 [PubMed: 21833026]

Xu C, Tian H, Sun H, Jiao Z, Zhang Y, Chen X, 2015a. A pH sensitive co-delivery system of siRNA and doxorubicin for pulmonary administration to B16F10 metastatic lung cancer. RSC Adv. 5, 103380–103385. 10.1039/c5ra21934e

Xu C, Wang P, Zhang J, Tian H, Park K, Chen X, 2015b. Pulmonary codelivery of doxorubicin and siRNA by pH-Sensitive nanoparticles for therapy of metastatic lung cancer. Small 11, 4321–4333. 10.1002/smll.201501034 [PubMed: 26136261]

Xu PY, Kankala RK, Pan YJ, Yuan H, Wang S Bin, Chen AZ, 2018. Overcoming multidrug resistance through inhalable siRNA nanoparticles-decorated porous microparticles based on supercritical fluid technology. Int. J. Nanomedicine 13, 4685–4698. 10.2147/IJN.S169399 [PubMed: 30154654]

Xue W, Dahlman JE, Tammela T, Khan OF, Sood S, Dave A, Cai W, Chirino LM, Yang GR, Bronson R, Crowley DG, Sahay G, Schroeder A, Langer R, Anderson DG, Jacks T, 2014a. Small RNA combination therapy for lung cancer. Proc. Natl. Acad. Sci. U. S. A 10.1073/pnas.1412686111

Xue W, Dahlman JE, Tammela T, Khan OF, Sood S, Dave A, Cai W, Chirino LM, Yang GR, Bronson R, Crowley DG, Sahay G, Schroeder A, Langer R, Anderson DG, Jacks T, 2014b. Small RNA combination therapy for lung cancer. Proc. Natl. Acad. Sci. U. S. A 111, 3553–3561. 10.1073/pnas.1412686111

Youngren-ortiz SR, Gandhi NS, Mahavir B, Street K, Program ET, Cancer T, 2017. Aerosol Delivery of siRNA to the Lungs. Part 2: Nanocarrierbased Delivery Systems. KONA Powder Part. J 34, 44–69. 10.14356/kona.2017005.Aerosol

Yue C, Liu P, Zheng M, Zhao P, Wang Y, Ma Y, Cai L, 2013. IR-780 dye loaded tumor targeting theranostic nanoparticles for NIR imaging and photothermal therapy. Biomaterials 34, 6853–6861. 10.1016/j.biomaterials.2013.05.071 [PubMed: 23777910]

Zeng J, Chen X, Liang Q, Xu X, Jing X, 2004. Enzymatic degradation of poly(L-lactide) and poly(epsilon-caprolactone) electrospun fibers. Macromol. Biosci 4, 1118–1125. 10.1002/mabi.200400092 [PubMed: 15586389]

Zhang K, Xu L, Jiang J, Calin N, Lam K, Zhang S, 2013. Facile Large-Scale Synthesis of Monodisperse Mesoporous Silica Nanospheres with Tunable Pore Structure Facile Large-Scale Synthesis of Monodisperse Mesoporous Silica Nanospheres with Tunable Pore Structure. J. Am. Chem. Soc 135, 2427–2430. 10.1021/ja3116873 [PubMed: 23363241]

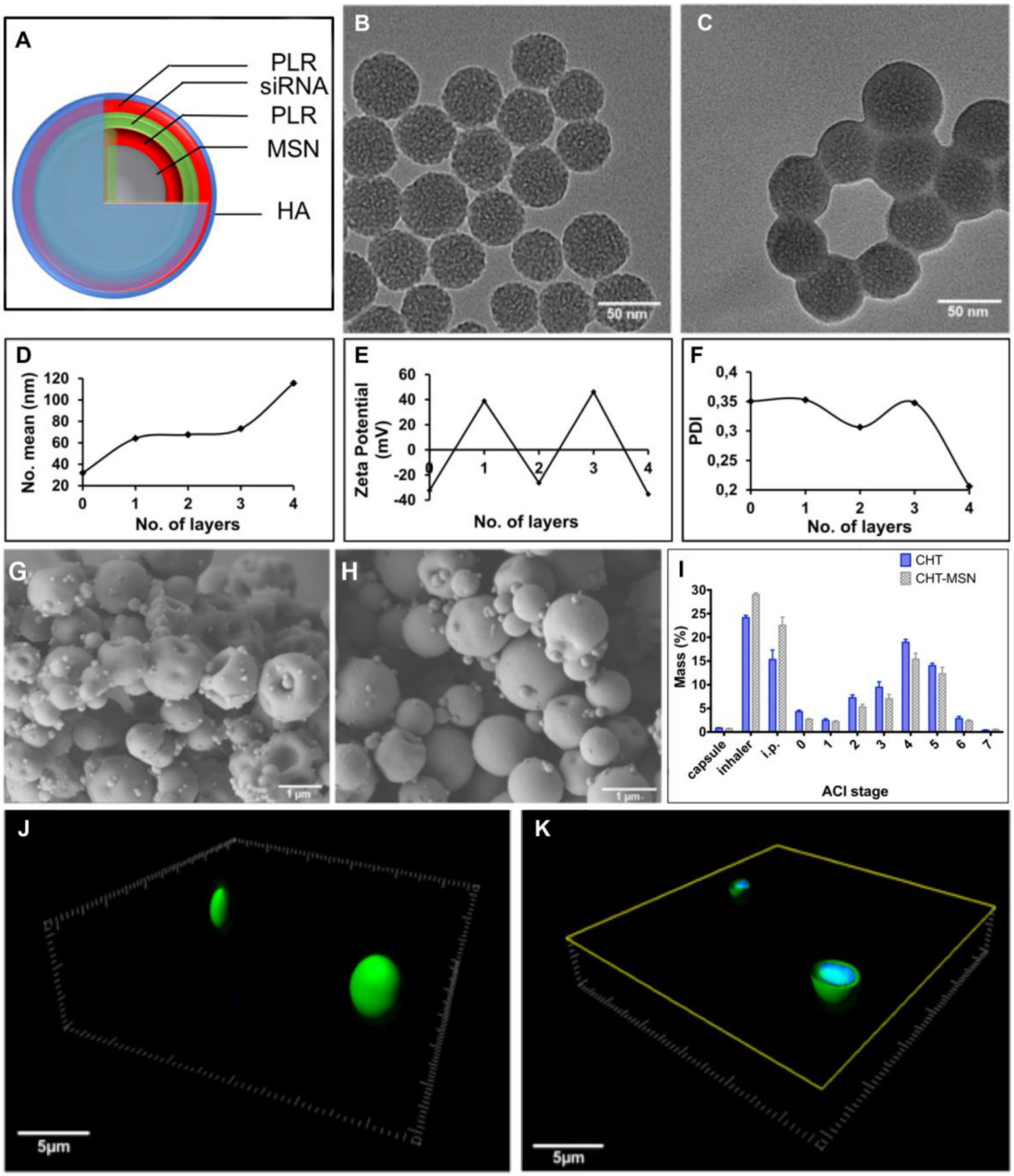

Figure 1.

Synthesis and characterization of aerosolized LbL nanoparticles. (A) Schematic representation siRNA-containing LbL nanoparticles. TEM images of (B) MSN's loaded with IR-780 dye and (C) siRNA LbL nanoconstructs from MSN cores, scale bars 50nm. (D) hydrodynamic diameter, (E) zeta potential, and (F) polydispersity index (PDI) of the LbL nanosystems. SEM images of the chitosan microparticles containing LbL nanoparticles in A-F: (G) CHT (x 16,000); (H) CHT-LbL siRNA (x 30,000), scale ba–s - 1m. (I) Powder dispersion among the micronized powders by ACI. 3D reconstruction of CHT-LbL siRNA micronized powders and (J) their cross-section image (K). Green: AF 488 siRNA (λ_{exc} =

473 nm; λ_{emm} = 520 nm); Blue – DAPI, CHT autofluorescence (λ_{exc} = 405 nm; λ_{emm} = 461 nm), scale bar - 5μm.

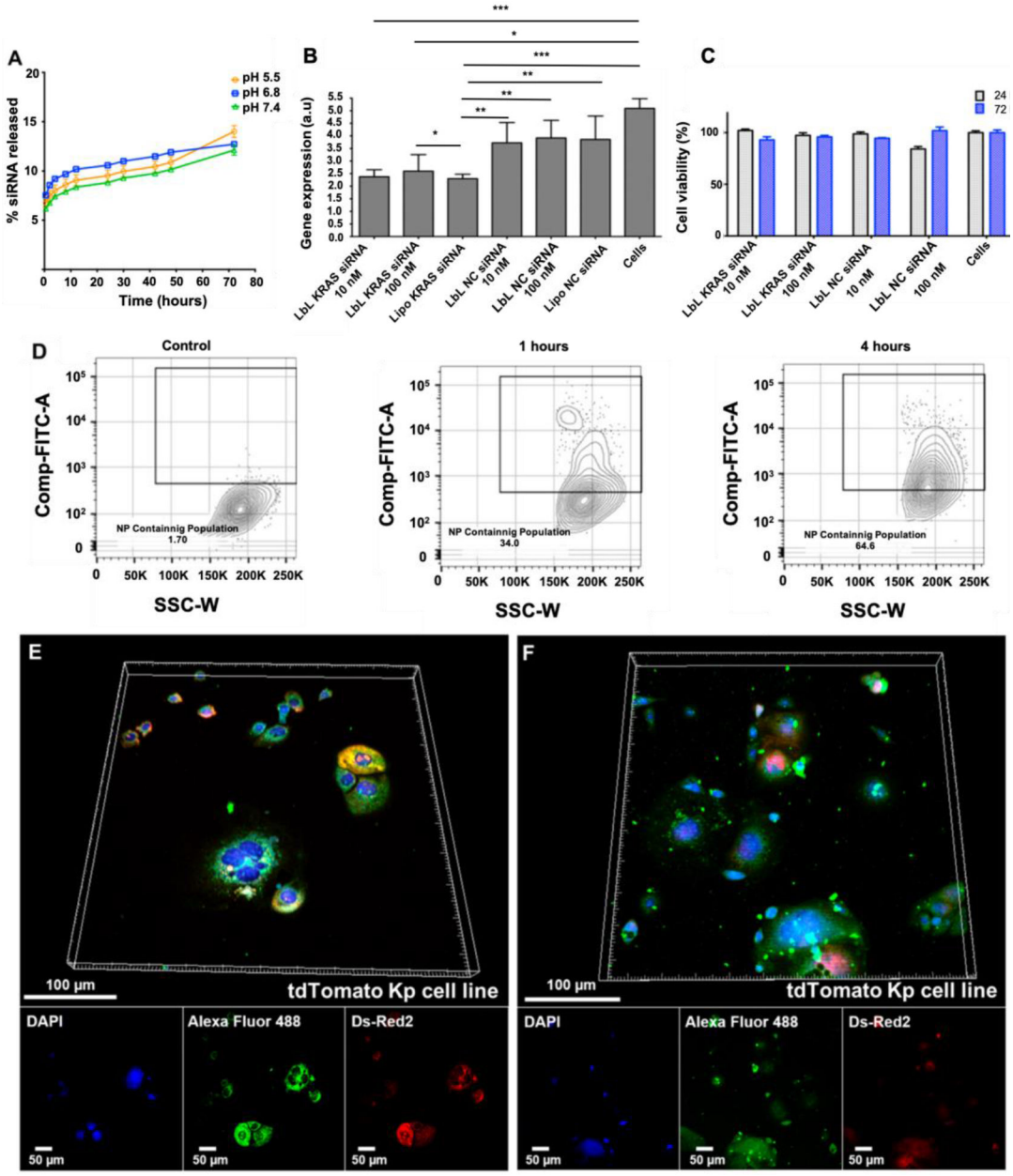

Figure 2.

Drug release and cellular interactions of LbL nanoparticles. (A) siRNA release from LbL nanoconstructs; (B) Gene expression of KRAS in tdTomato–expressing KP cell line; (C) Cell viability of tdTomato-expressing KP cells 24 and 72 h after contact with the engineered LbL nanosystems; (D) FACs analysis of nanoparticle uptake after 1 and 4 hours; CLSM images of td Tomato expressing KP cells incubated with the LbL siRNA nanoparticles and 3D reconstruction after (E) 1 and (F) 4h. Ch1 – Hoechst, nuclear location (λ_{exc} = 405 nm ; λ_{emm} = 461 nm); Ch2 – AF 488, siRNA (λ_{exc} = 463 nm ; λ_{emm} = 520 nm); Ch3 – Ds-Red2, tdTomato Kp cell line (λ_{exc} = 559 nm ; λ_{emm} = 581 nm). *P < 0.05; **P < 0.01; ***P < 0.001

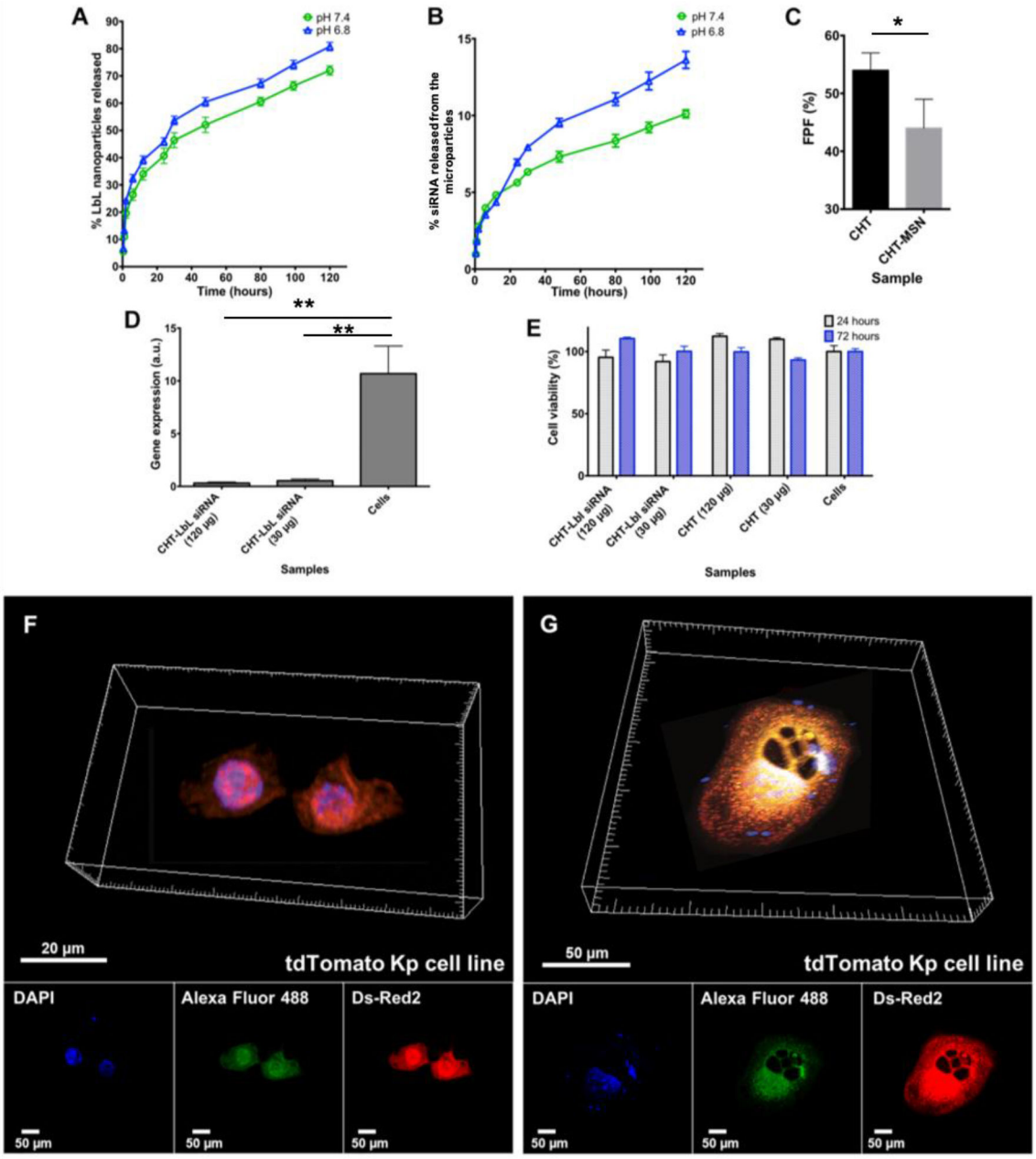

Figure 3.

Drug release and cellular interactions of aerosolizable nano-in-micro particles. Release assays of (A) LbL nanoparticles from micronized powders; (B) siRNA from micronized powders; (C) Percentage of Fine Particle Fraction (FPF %) of the micronized powders; (D) Effects of CHT-LbL siRNA microparticles on KRAS gene expression in tdTomato–expressing KP cell line (72 h); (E) Cell viability of tdTomato–expressing KP cell line in the presence of micronized powders; CLSM of td Tomato expressing KP cell line incubated with the LbL siRNA microparticles and 3D reconstruction after (F) 1 and (G) 12 h. Ch1 – DAPI, microparticles and proteins autofluorescence (λ_{exc} = 405 nm ; λ_{emm} = 461 nm); Ch2

– AF 488, siRNA (λ_{exc} = 473 nm ; λ_{emm} = 520 nm); Ch3 – Ds-Red2, tdTomato Kp cell line (λ_{exc} = 559 nm ; λ_{emm} = 581 nm). *P < 0.05; **P < 0.01; ***P < 0.001

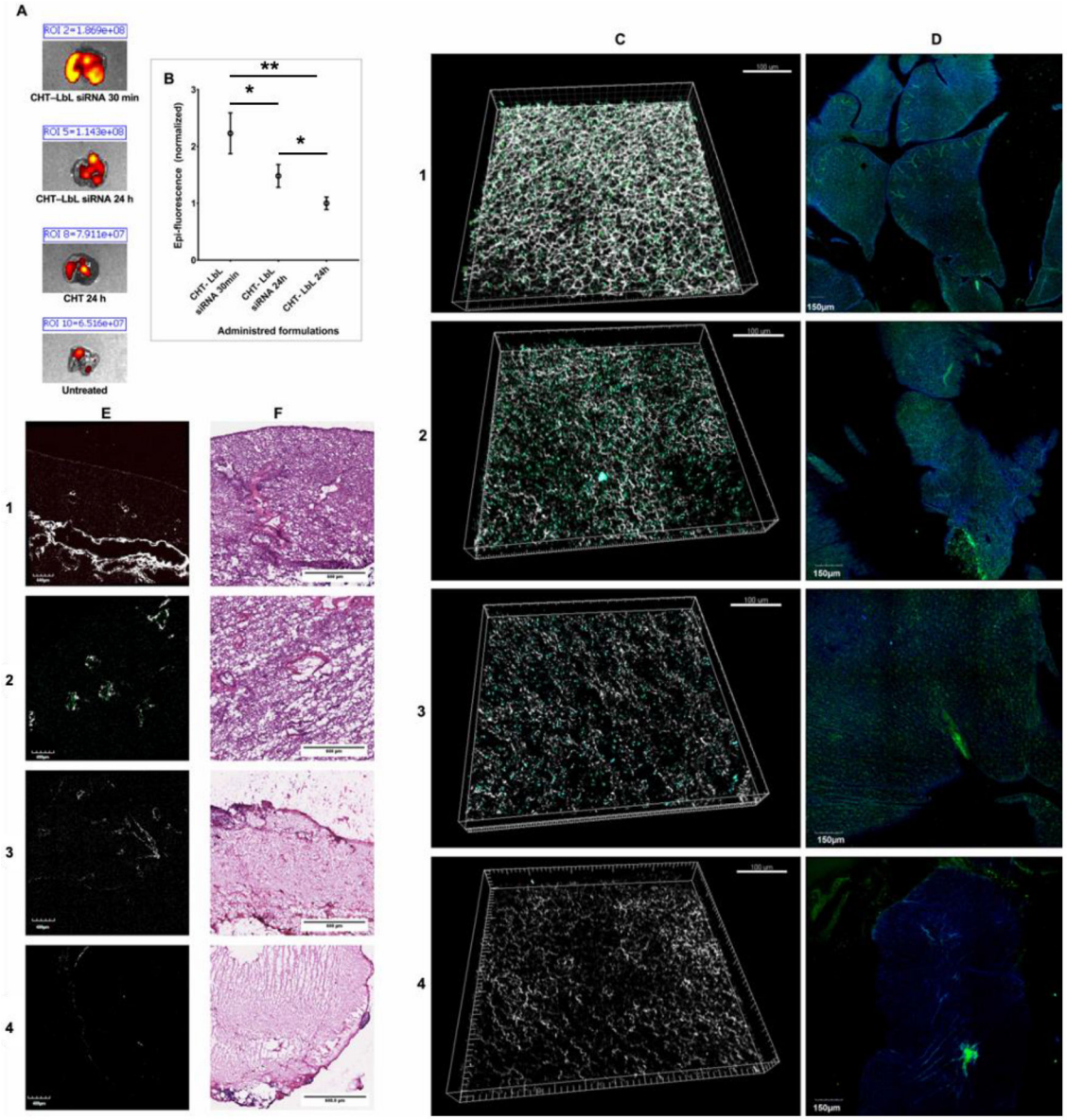

Figure 4.

Pulmonary delivery from aerosolized LbL nano-in-micro particles. Micronized powder biodistribution in mice lungs: (A) Accumulation of the particles in mice lungs over pre-determined periods of time (λ_{exc} = 465 nm; λ_{emm} = 520 nm); (B) Region-of- interest (ROI) analysis of lungs-specific accumulation. Histological analysis of extracted lungs: (1) CHT-LbL siRNA 30 min; (2) CHT-LbL siRNA 24 h; (3) CHT 24 h; (4) Untreated of (E) unstained and (F) H&E stained lung tissue sections isolated from the mice. E was imaged with a Nikon light microscope (4x) and F was imaged using TPCM (using a 25x, N.A. 1.05 objective at 840 nm). *P < 0.05; **P < 0.01; ***P < 0.001

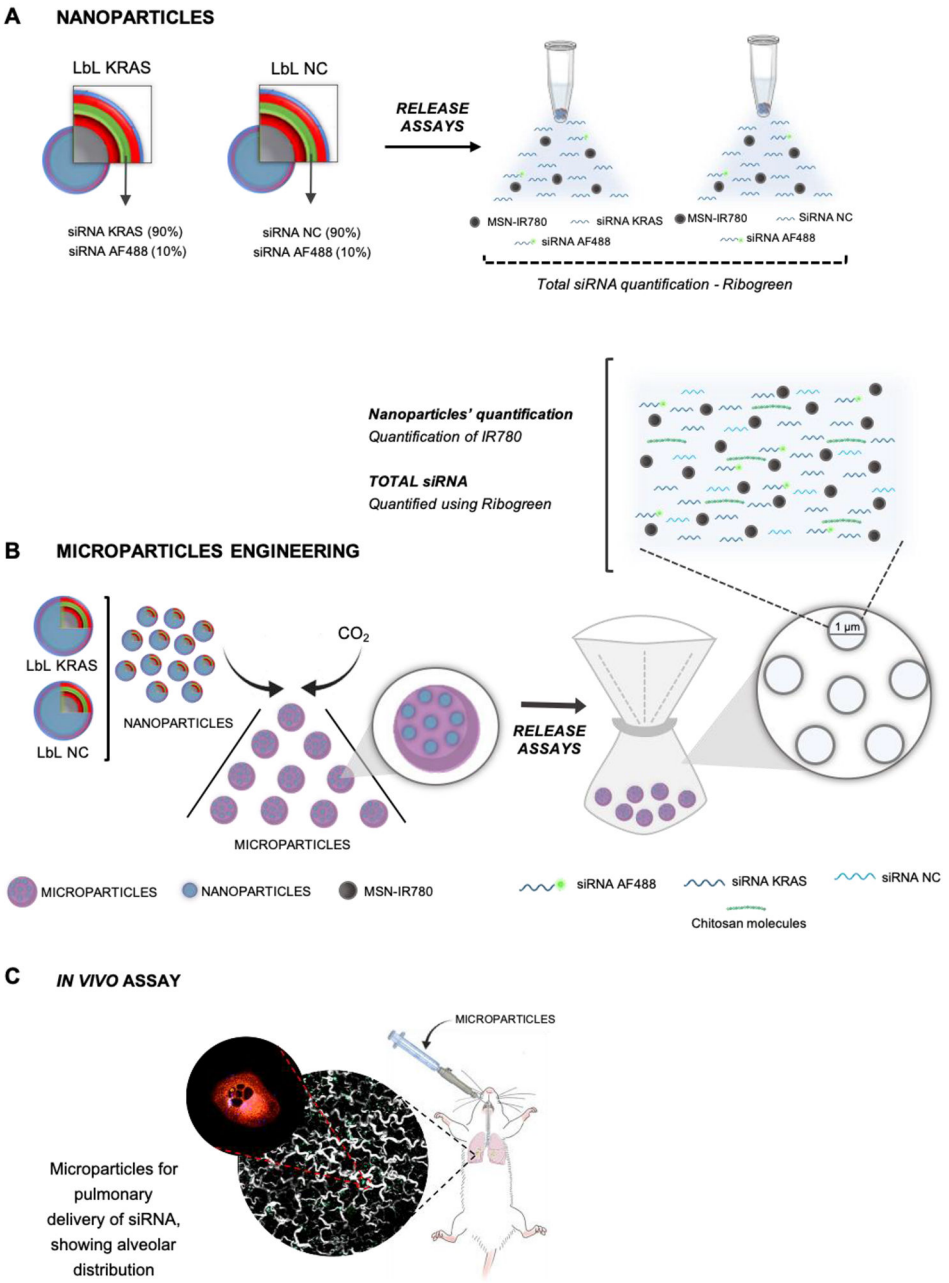

Scheme 1 –.

Schematic representation of the developed assays: A- Nanoparticles schematic representation, and illustrative demonstrating of siRNA release from the nanodevices, measured by the Riboreen assay; B – Graphical represenation of microparticles engineering. The release of nanoparticles and siRNA from the micropowders was also quantified by measuring the IR-780 and thorugh the Ribogreen assay, respectively; C – *In vivo* assay representation: Pulmonary administration of the micropowders and its alveolar distribution

Table 1 -

siRNA deposition onto LbL nanosystems

5 mg of MSN_IR-780	siRNA (initial amount)	Encapsulation efficiency - total siRNA	Percentage of AF 488 siRNA in total siRNA	Percentage of AF 488 siRNA in LbL nanoparticles
After siRNA layering	≈ 2040 μg (120 nmol of siRNA Kras or NC + 16 nmol of AF 488 siRNA)	11.4 % = 232.2 μg	1.2 % of initial siRNA = 25.1 μg	10.8%
After enzymes degradation		10.7 % = 219.1 μg	1.1 % of initial siRNA = 23.3 μg	10.6%

Table 2.

IR-780 dye and siRNA encapsulation (EE%) and entrapment efficiencies (E%)[a]

IR-780 dye initial amount	IR-780 dye within LbL nanosystems (EE%)	IR-780 dye within nano-in-micro formulations (E%)	siRNA (μg) within nano-in-micro formulations	Total amount of siRNA in 1.5 mg of powder (μg)	siRNA Kras in 1.5mg of powder (ug)[c]
0.13 mg/mL	82.2%: 0.1 mg/mL	28.7%: 0.03 mg/mL (in 71.9 mg of powder)	133.4 μg (in 71.9 mg of powder) – 28.7%[b]	2.8 μg	1.25 ug

[a] EE% was calculated as E%. Nevertheless, the last one considers the possibility of entrapment at the surface of the microparticles.

[b] Initial amount of LbL nanoparticles in the CHT mixture: 10 mg which is approximately 464.4ug of siRNA

[c] CHT-LbL nanoparticles: 50% LbL siRNA Kras (with 89.3% siRNA Kras) + 50% LbL siRNA NC ⇒ % of siRNA Kras in CHT-LbL nanoparticles ≈ 44.65%